Damping of Offshore Wind Turbine Tower Vibrations by a Stroke Amplifying Brace

Brodersen, Mark Laier; Høgsberg, Jan Becker

Published in:
Energy Procedia

Link to article, DOI:
10.1016/j.egypro.2014.07.235

Publication date:
2014

Document Version
Publisher's PDF, also known as Version of record

Available online at www.sciencedirect.com

ScienceDirect

Energy Procedia 53 (2014) 258 – 267

Energy Procedia

EERA DeepWind'2014, 11th Deep Sea Offshore Wind R&D Conference

Damping of offshore wind turbine tower vibrations by a stroke amplifying brace

Mark L. Brodersen, Jan Høgsberg

Department of Mechanical Engineering, Technical University of Denmark, DK-2800 Lyngby, Denmark

Abstract

The potential of installing dampers inside the tower of an offshore wind turbine is investigated through simulations. Dampers are installed at the bottom to act on the curvature of the tower, and it is shown that dampers installed in suitable braces have the potential to increase the critical damping ratio of the two lowest tower modes by 1 percent. By using a toggle-brace system, damper stroke is increased, while the damper force is reduced. Finally, by installing the dampers in a symmetric configuration, tuning for maximum damping is approximately independent of the orientation of the rotor, thereby making this installation of dampers feasible.

Selection and peer-review under responsibility of SINTEF Energi AS
Keywords: Stroke amplifying toggle brace, Passive damping, Fixed offshore wind turbine

Introduction

Design of monopile support structures for large offshore wind turbines, as the wind turbine illustrated in figure 1, is usually driven by fatigue. Due to the relatively low inherent damping of cross-wind tower vibrations, the fatigue lifespan is significantly influenced by cross-wind vibrations caused by wave loading misaligned with the wind [1]. In the future larger offshore wind turbines will be operating at larger water depths, whereby the critical tower frequency will be lowered and potentially approach the excitation frequency of the waves. This may cause fatigue damage due to wave loading to increase significantly, whereby the monopile support structure may reach its limit of structural feasibility. A way to extend the feasibility of the monopile support structure is by means of structural control, in which external devices are installed in order to reduce the dynamic response.

For structural control of fixed offshore wind turbines, resonant damping is the concept most widely used by the industry [1], and it is also the damping concept that has received the most attention in the literature. Installation of a resonant damper like a Tuned Liquid Damper (TLD) or a Tuned Mass Damper (TMD) have been shown to lead to a reduction of the fatigue damage accumulated in the monopile of an offshore wind turbine [2,3]. In order to be effective

* Corresponding author. Tel.: +45 4525 1377 ; fax: +45 4588 4325.
E-mail address: mlai@mek.dtu.dk

Selection and peer-review under responsibility of SINTEF Energi AS
doi:10.1016/j.egypro.2014.07.235

a resonant damper like a TMD should be installed where the absolute motion of the targeted vibration mode is large, which is at the top of the tower or inside the nacelle. However, with a TMD efficient damping is associated with large damper motion and large damper mass, which is highly undesirable and maybe even unfeasible at the top of a slender wind turbine tower. In order to avoid these installation issues, a concept with semi-active dampers installed in a stroke amplifying toggle-brace-damper system inside the tower has been proposed by Fischer et al. [4]. The brace is installed in order to amplify the horizontal relative motion of the tower walls to a larger displacement of the damper. A toggle-brace system is a well known concept for application in shear frames [5], where it is used to amplify the horizontal drift of the frame to a larger displacement over the damper. This has been proven to enhance the energy dissipation of a damper installed in a shear frame, when compared to the same damper installed using a traditional diagonal brace [6]. Likewise, the present paper considers installation of passive dampers to act on the relative motion of the tower, though using a more realistic model for the tower wall deflection, that takes into account both horizontal and vertical displacements of the tower walls.

A passive damper is by definition collocated, which means that the two concepts of controllability and observability fuse together. In this paper the two concepts are represented in the term 'modal connectivity'. Critical for the effective implementation of passive dampers inside the tower is sufficient damper stroke and sufficient attainable damping, both related to modal connectivity. The damper stroke is represented by the displacement of the damper with respect to the targeted vibration form, while attainable damping is associated with the ability of the damper to change the natural frequency of the structure when the damper is locked [7]. Vibrations of the tower are dominated by a combination of the two lowest tower modes, fore-aft mode and side-to-side mode, as seen in figure 2 and figure 3, respectively. This means that both modes need to be addressed. In the two modes the tower is primarily deformed in bending, while rotor, nacelle and blades act as lumped inertia at the free end of the tower. Modal connectivity is maximized, by positioning the dampers at the bottom of the tower, where the curvature associated with bending is largest. Although the modal connectivity is maximized, the displacement of the damper is likely to be small, thereby making installation of passive dampers inside the tower unfeasible. In order to increase the displacement of the damper and thereby the feasibility of installing passive dampers inside the tower, a toggle-brace-damper concept is introduced. The toggle-brace concept amplifies the relative displacement of the tower to a larger displacement of the damper, whereby at the same time the damper force is decreased.

Another important aspect of installing passive dampers inside the tower is the relative circumferential positioning of the dampers. Since the wind turbine rotor can turn relative to the tower, dampers should be positioned in a layout so that damping is independent of the position of the rotor. In this paper it will be demonstrated that equally tuned dampers can be positioned in a circumferential symmetric layout, so that the damping ratio of the two lowest tower modes remain approximately constant with respect to the orientation of the rotor.

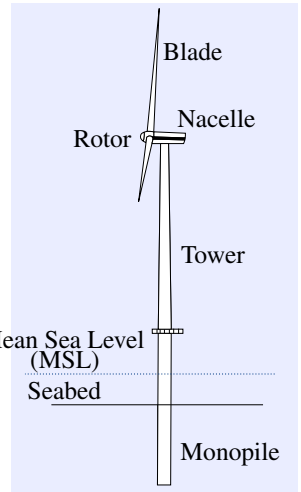

Fig. 1. Offshore wind turbine

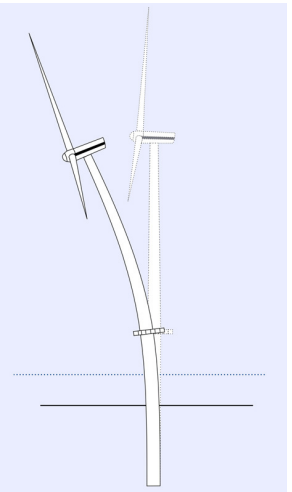

Fig. 2. Fore-aft mode

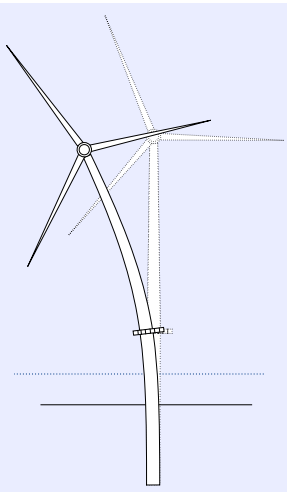

Fig. 3. Side-to-side mode

Modelling of wind turbine with brace damper concept

Due to the slender geometry of the tower and blades, the structural dynamics of a wind turbine is commonly described using a non-linear numerical beam model. For a simple assessment of the influence of the brace damper system a linear model is however convenient. A simple linear beam model is obtained by assuming the wind turbine to be at standstill, by representing the inertia of the rotor, nacelle and blades as lumped inertia at the top of the tower and by modeling the flexible foundation of the soil using a linear Winkler type spring model.

The beam model, as illustrated in figure 4, is defined with the global y-axis in the direction of the rotor, the global x-axis in the direction perpendicular to the rotor, and the global z-axis in the vertical tower direction. A part of the beam model from node n to node $n+2$ is illustrated in figure 5. Each node in the beam model carries six degrees of freedom (dofs), three translations $\mathbf{u}_n^T = [u_x, u_y, u_z]$ and three rotations $\boldsymbol{\varphi}_n^T = [\varphi_x, \varphi_y, \varphi_z]$ all defined with respect to the global coordinate system of the beam model. The discretized equations of motion are given in terms of the nodal displacement vector $\mathbf{u}$ as

$$\mathbf{M}\ddot{\mathbf{u}} + \mathbf{C}\dot{\mathbf{u}} + \mathbf{K}\mathbf{u} = \mathbf{f}_d + \mathbf{f}_{ext}, \tag{1}$$

where $\mathbf{M}$ is the mass matrix, $\mathbf{K}$ is the stiffness matrix, $\mathbf{C} = \alpha\mathbf{M} + \beta\mathbf{K}$ is a proportional damping matrix to represent structural damping, $\mathbf{f}_d$ is the nodal load vector due to external dampers, and $\mathbf{f}_{ext}$ is the generalized forces associated with external loads due to wind and waves. The stiffness matrix $\mathbf{K} = \mathbf{K}_e + \mathbf{K}_s$ consist of two parts: The usual constitutive elastic stiffness matrix $\mathbf{K}_e$ and the stiffness matrix for the elastic foundation $\mathbf{K}_s$. $\mathbf{K}_e$ is based on the complementary energy principle following Krenk [8], whereby both extension, bending, shear and torsion deformations are included in the element formulation. The specific implementation of the element stiffness matrix follows Svendsen [9].

Damper implementation

Two different implementations of dampers are considered. The first implementation, with two dampers installed on opposite walls of the tower to act directly on the curvature of the tower, is shown in figure 6(a). In this paper this implementation is referred to as a curvature-brace. In the figure θ_2 describes the angle between the tower wall and the horizontal direction and θ_3 describes the circumferential angle between the global x-axis and the direction of the damper, which will change as the position of the rotor relative to the tower changes. When $\theta_3 = 0°$ and $\theta_3 = 180°$ the damper will only influence the side-to-side mode, while when $\theta_3 = 90°$ and $\theta_3 = 270°$ the damper will only influence the fore-aft mode. Figure 6(b) shows several braces installed in a homogeneously distributed circumferential layout with 60° between the orientation of each damper, in order for the combined curvature-brace system to be able to damp vibrations in any direction.

In spite of a large modal connectivity, the feasibility of a curvature-brace system is limited by the relatively small displacement over the dampers. To overcome this and thereby improve the feasibility, another implementation is considered, where dampers are installed in a curvature-toggle-brace, as shown in figure 6(c). Compared to the curvature-brace, the relative displacement of the tower is amplified to a larger displacement over the damper, by the use of a toggle mechanism. Attainable damping for the curvature-toggle-brace is expected to be the same as for the curvature brace. At one end the damper is connected to the toggle mechanism, while at the other end the damper is connected to a joint, which must be kept at the centerline of the tower cross section by e.g. a number of additional supporting braces. The geometry of the toggle-brace is described entirely in terms of the angle θ_1 between the brace and the tower wall, the angles θ_2 and θ_3, and the radius r of the tower. Minimizing θ_1 will maximize the amplification of the toggle brace, while the distance of the toggle joint to the tower wall should be large enough to avoid snap-through during operational conditions. In this paper the angle is fixed at $\theta_1 = 5°$. Figure 6(d) shows several braces in a curvature-toggle-brace system installed in a homogeneously distributed circumferential layout, with 60 ° between each damper.

Connectivity vector

The influence of installing a damper in the wind turbine tower is in the beam model described by its connectivity vector $\mathbf{w}$ and the magnitude of the damper force f_d, whereby the force vector is given as

$$\mathbf{f}_d = -\mathbf{w} f_d \tag{2}$$

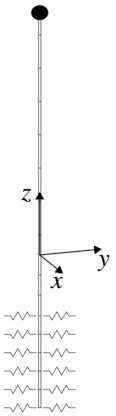

Fig. 4. Beam model

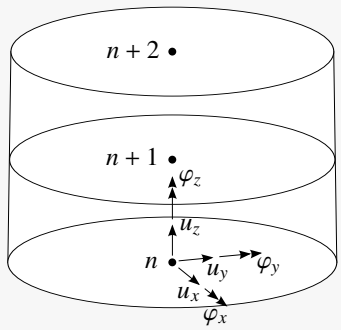

Fig. 5. Section of beam model

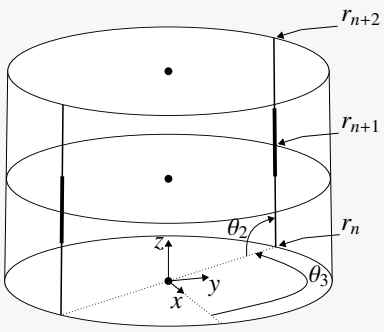

(a)

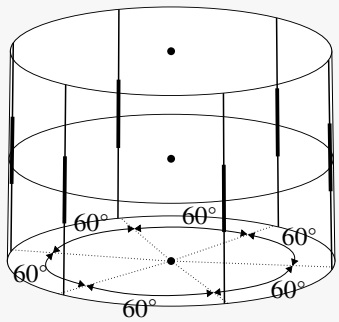

(b)

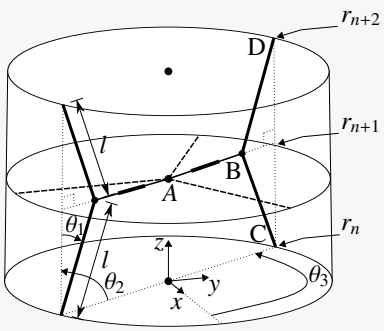

(c)

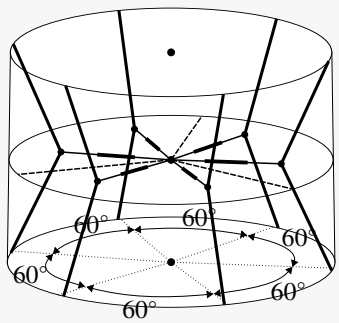

(d)

Fig. 6. (a) Curvature brace, (b) Curvature brace system, (c) Curvature toggle brace and (d) Curvature toggle brace system

The connectivity vector **w** transforms the forces and moments imposed by the damper on the tower into equivalent nodal forces in the beam model. In this sense **w** describes the connection of the damper to the tower structure through the brace mechanism, whereby in this context it may be seen as an extension of the magnification factor used for design of toggle-brace concepts in shear frames [5]. If the damper and connectivity vector are both assumed to operate linearly, the displacement of the damper u_d is given by

$$u_d = \mathbf{w}^T \mathbf{u} \tag{3}$$

Equation (3) implies that the brace members are rigid. The connectivity vector is determined by computing the nodal load vector imposed by the brace-damper system on the beam model representing the tower, with each damper considered separately. When the toggle-brace is connected to the tower centerline, it results in apparent nodal forces, whereas when the brace is connected to the tower wall, it leads to nodal forces as well as nodal moments.

As an example, consider the damper associated with member AB in figure 6(c). Each member of the brace acts as a bar, only allowing axial bar forces. The bar force N_{AB} in member AB is directly given as the damper force f_d, and due to symmetry, the bar force in member BC, N_{BC}, equals the bar force in member BD, N_{BD}, whereby force equilibrium of joint B gives

$$N_{BC} = N_{BD} = \frac{1}{2}\frac{f_d}{\sin\theta_1} \tag{4}$$

When assuming $\cos\theta_1 \simeq 1$, the nodal load vectors for the nodes n, $n+1$ and $n+2$ follow as

$$\mathbf{f}_{d,n} = \begin{bmatrix} -\frac{1}{2}\cos\theta_3\left(\frac{\cos\theta_2}{\sin\theta_1}+\sin\theta_2\right) \\ -\frac{1}{2}\sin\theta_3\left(\frac{\cos\theta_2}{\sin\theta_1}+\sin\theta_2\right) \\ \frac{1}{2}\left(\frac{\sin\theta_2}{\sin\theta_1}-\cos\theta_2\right) \\ \frac{1}{2}r_n\sin\theta_3\left(\frac{\sin\theta_2}{\sin\theta_1}-\cos\theta_2\right) \\ -\frac{1}{2}r_n\cos\theta_3\left(\frac{\sin\theta_2}{\sin\theta_1}-\cos\theta_2\right) \\ 0 \end{bmatrix} f_d, \quad \mathbf{f}_{d,n+1} = \begin{bmatrix} \cos\theta_3\sin\theta_2 \\ \sin\theta_3\sin\theta_2 \\ \cos\theta_2 \\ 0 \\ 0 \\ 0 \end{bmatrix} f_d, \quad \mathbf{f}_{d,n+2} = \begin{bmatrix} \frac{1}{2}\cos\theta_3\left(\frac{\cos\theta_2}{\sin\theta_1}-\sin\theta_2\right) \\ \frac{1}{2}\sin\theta_3\left(\frac{\cos\theta_2}{\sin\theta_1}-\sin\theta_2\right) \\ -\frac{1}{2}\left(\frac{\sin\theta_2}{\sin\theta_1}+\cos\theta_2\right) \\ -\frac{1}{2}r_{n+2}\sin\theta_3\left(\frac{\sin\theta_2}{\sin\theta_1}+\cos\theta_2\right) \\ \frac{1}{2}r_{n+2}\cos\theta_3\left(\frac{\sin\theta_2}{\sin\theta_1}+\cos\theta_2\right) \\ 0 \end{bmatrix} f_d \tag{5}$$

The three linearized connectivity vectors for nodes n to $n+2$ are now obtained from (2) as

$$\mathbf{w}_n = \begin{bmatrix} \frac{1}{2}\cos\theta_3\left(\frac{\cos\theta_2}{\sin\theta_1}+\sin\theta_2\right) \\ \frac{1}{2}\sin\theta_3\left(\frac{\cos\theta_2}{\sin\theta_1}+\sin\theta_2\right) \\ -\frac{1}{2}\left(\frac{\sin\theta_2}{\sin\theta_1}-\cos\theta_2\right) \\ -\frac{1}{2}r_n\sin\theta_3\left(\frac{\sin\theta_2}{\sin\theta_1}-\cos\theta_2\right) \\ \frac{1}{2}r_n\cos\theta_3\left(\frac{\sin\theta_2}{\sin\theta_1}-\cos\theta_2\right) \\ 0 \end{bmatrix}, \quad \mathbf{w}_{n+1} = \begin{bmatrix} -\cos\theta_3\sin\theta_2 \\ -\sin\theta_3\sin\theta_2 \\ -\cos\theta_2 \\ 0 \\ 0 \\ 0 \end{bmatrix}, \quad \mathbf{w}_{n+2} = \begin{bmatrix} -\frac{1}{2}\cos\theta_3\left(\frac{\cos\theta_2}{\sin\theta_1}-\sin\theta_2\right) \\ -\frac{1}{2}\sin\theta_3\left(\frac{\cos\theta_2}{\sin\theta_1}-\sin\theta_2\right) \\ \frac{1}{2}\left(\frac{\sin\theta_2}{\sin\theta_1}+\cos\theta_2\right) \\ \frac{1}{2}r_{n+2}\sin\theta_3\left(\frac{\sin\theta_2}{\sin\theta_1}+\cos\theta_2\right) \\ -\frac{1}{2}r_{n+2}\cos\theta_3\left(\frac{\sin\theta_2}{\sin\theta_1}+\cos\theta_2\right) \\ 0 \end{bmatrix}, \tag{6}$$

The connectivity vector for the full brace is obtained by assembling the nodal vectors in (6) as

$$\mathbf{w}^T = \begin{bmatrix} \dots & \mathbf{w}_n^T & \mathbf{w}_{n+1}^T & \mathbf{w}_{n+2}^T & \dots \end{bmatrix}^T, \tag{7}$$

The total load vector associated with several braces in a collective damping system is given by the summation

$$\mathbf{f}_d = \sum_k^N \mathbf{f}_{d,k}, \tag{8}$$

where N denotes the total number of damper braces in the circumferential direction.

Influence of external damping system

The dampers in the damper-brace system are assumed to be viscous dampers with *a single* common viscous damping parameter c. When expressing the damper force from each damper $f_{d,k}$ in the frequency domain as

$$f_{d,k} = i\, c\, \omega\, u_{d,k}, \tag{9}$$

the contribution from the external damping system is

$$\mathbf{f}_d = -i\, \omega\, c\, \sum_k^N \mathbf{w}_k \mathbf{w}_k^T \mathbf{u}, \tag{10}$$

where N again denotes the total number of damper-braces in the circumferential direction. Setting $\mathbf{f}_{ext} = \mathbf{0}$, neglecting structural damping, $\mathbf{C} = \mathbf{0}$, and substituting (10) into the frequency representation of (1), gives the frequency equation of motion for the combined tower and damping system

$$\left(\mathbf{K} - \omega^2 \mathbf{M} + i\, \omega\, c\, \sum_k \mathbf{w}_k \mathbf{w}_k^T\right)\mathbf{u} = 0, \tag{11}$$

from which the eigenfrequencies ω, associated with the side-to-side and the fore-aft mode, of the combined system are determined in the following section. For vanishing damping parameter ($c = 0$) the frequency equations of motion of the undamped structure is recovered

$$\left(\mathbf{K} - \omega_0^2 \mathbf{M}\right)\mathbf{u}_0 = 0 \tag{12}$$

For infinite damping parameter ($c \to \infty$) the dampers are locked, leading to the frequency equation for another undamped system

$$\left(\mathbf{K} - \omega_\infty^2 \mathbf{M}\right)\mathbf{u}_\infty = \mathbf{r} \tag{13}$$

where $\mathbf{r} = \mathbf{w}\, r$ is the reaction vector given in terms of the reaction force r required to lock the dampers.

Two component representation for a single frequency

The frequency of the side-to-side mode and for-aft mode are dealt with separately, by describing the combined system with tower and dampers in a two-component representation as proposed in [7]. In this simplified approach the full state $\mathbf{u}$ is projected on to a subspace expanded by the two limiting real valued mode shapes, $\mathbf{u}_0$ from (12), and $\mathbf{u}_\infty$ from (13), whereby

$$\mathbf{u} = \mathbf{u}_0 \xi_0 + \mathbf{u}_\infty \xi_\infty, \tag{14}$$

with ξ_0 and ξ_∞ as the corresponding modal amplitudes. From (14) an approximate explicit formula for the frequency ω of the combined system can be derived, see [10], as

$$\frac{\omega - \omega_0}{\omega_\infty - \omega_0} = \frac{\Delta\omega}{\Delta\omega_\infty} \simeq \frac{i\eta}{1 + i\eta}, \tag{15}$$

where η is a non-dimensional damping parameter

$$\eta = \frac{\omega_0\, c}{\omega_\infty^2 - \omega_0^2} \sum_k^N \gamma_k^2 = \frac{\omega_0 c}{\omega_\infty^2 - \omega_0^2}\gamma^2, \tag{16}$$

given by the cumulative sum, $\gamma^2 = \sum_k^N \gamma_k^2$, of the displacement of each damper $\gamma_k = \mathbf{w}_k^T \mathbf{u}_0$, as the mode shape $\mathbf{u}_0$ has been normalized to unit modal mass, $\mathbf{u}_0^T \mathbf{M} \mathbf{u}_0 = 1$. The relation in (15) for the relative frequency increment has a general character. It describes a semi-circular trajectory in the complex plane, which for $\eta = 1$ gives a maximum value for the imaginary part

$$\frac{\Delta\omega}{\Delta\omega_\infty} = \frac{i}{1 + i} \qquad \Rightarrow \qquad \mathrm{Im}[\Delta\omega] = \mathrm{Im}[\omega] = \frac{1}{2}\Delta\omega_\infty \tag{17}$$

This point corresponds to maximum attainable damping. The complex valued natural frequency is described in terms of the damping ratio ζ as

$$\omega = |\omega|\left(\sqrt{1-\zeta^2} + i\zeta\right), \tag{18}$$

whereby the damping ratio is given by

$$\zeta = \frac{\mathrm{Im}[\omega]}{|\omega|} \tag{19}$$

Maximum attainable damping follows from insertion of (17), whereby

$$\zeta_{max} = \frac{\Delta\omega_\infty}{2|\omega|} \simeq \frac{\Delta\omega_\infty}{\omega_0 + \omega_\infty}, \tag{20}$$

where $2|\omega| \simeq \omega_0 + \omega_\infty$ has been used to obtain the last expression. From (20) it is clear that attainable damping only depends on the change in frequency caused by locking the damper. For lightly damped structures, damping of the structure and the damping introduced by the external dampers are approximately additive, and ζ_{max} is therefore the increase in damping. The optimum value for the viscous parameter, c_{opt}, is found from equation (16) by setting $\eta = 1$, whereby

$$c_{opt} = \frac{\omega_\infty^2 - \omega_0^2}{\omega_0 \gamma^2} \tag{21}$$

It is clearly seen that optimum tuning to get maximum damping is given as a ratio between the change in frequency associated with locking the dampers and the sum of the displacement across the dampers.

Numerical simulations

The objective of this numerical example is to demonstrate the performance of the curvature-brace and curvature toggle-brace in damping of tower vibrations of an offshore wind turbine. The study considers a reference wind turbine used in the Offshore Code Comparison Collaboration study (OC3) [11]. It consist of the 77.6 m tall land based NREL 5 MW reference wind turbine, mounted on a 66 m long monopile. Viscous dampers are installed at the bottom of the tower 10 m above mean sea level, in a circumferential symmetric setup with six dampers positioned 60 ° apart, as illustrated in figures (b) and (d) for the curvature-brace and curvature-toggle-brace. The damper system is 4 m high, the dampers all use the same viscous damping parameter, c, and the brace members are assumed rigid.

Damper displacement

Sufficient damper displacement is critical for the effective implementation of passive dampers inside the tower, in order to activate the damper and in order to reduce the damper force. The damper stroke with respect to the fore-aft and the side-to-side tower modes, is computed by equation (3) when assuming the tower top displacement in the two modes to be 0.5 m. The displacement of a damper u_d as function of the circumferential orientation of the damper,θ_3, is seen in figure 7. The figure shows a comparison between the damper installed in a curvature-brace (dotted and dashed) and the damper installed in a curvature-toggle-brace (dash-dotted and solid). The two different curves for each brace represent the displacement with respect to the fore-aft mode and the side-to-side mode, respectively. As expected the displacement varies with respect to θ_3 according to a sine function for the fore-aft mode and according to a cosine function for the side-to-side mode. When the damper is installed in the curvature-toggle-brace the displacement is seen to be larger compared to the damper installed in the curvature-brace.

Optimum tuning of the dampers is given by equation (21). For proper tuning it is therefore especially $\gamma^2 = \sum_k^N \gamma_k^2$, that is relevant. Values for γ^2 are plotted as function of the orientation of the rotor in figure 8. The figure shows curves for γ^2 for the curvature-brace (dotted and dashed) and for the curvature-toggle-brace (dash-dotted and solid) with respect to both the fore-aft mode and side-to-side mode. As expected γ^2 is larger for the curvature-toggle-brace than for the curvature-brace, leading to a smaller value for the optimum viscous parameter. For both braces the value of γ^2 is approximately constant with respect to the orientation of the rotor, indicating that one value for the viscous parameter will be close to optimum for any orientation of the rotor. Furthermore, the curves for the fore-aft mode and

the side-to-side mode are very similar. If attainable damping for the two modes are the same, the optimum viscous parameter for the two modes will therefore also be the same.

Root locus analysis

The development of a complex root of the frequency equation (11) approximately follows a semicircle in the complex plane as described by the expression in equation (15). Figure 9 shows the development of the roots associated with the fore-aft mode and the side-to-side mode, as the value of the viscous damping parameter c is increased. Figures 9(a) and (b) are for the curvature-brace and figures 9(c) and (d) are for the curvature-toggle-brace. The solid curve represents the theoretical expression (15) given by the non-dimensional damping parameter η in (16), while the dots are numerical values computed for an increasing value of c by solving (11). The values for c have been determined by appropriate tuning, according to (16), so that dots 1 to 10 correspond to the values of η going from 0 to 1 and dots 10 to 19 correspond to the values of η going from 1 to ∞. For both modes the tuning has been with respect to the side-to-side mode, which means that the values for c are the same in figures 9(a) and (b) and the same in figures 9(c) and (d). By comparing figures 9(a) and (b) for the curvature-brace and figures 9(c) and (d) for the curvature-toggle-brace, attainable damping with respect to the two different tower modes are seen to be very similar. Since the values for γ^2 for the two modes are the same, optimum tuning for the two modes is approximately the same. This is also seen by dot 10 being approximately at the maximum of both curves. Furthermore, attainable damping for the two braces is also seen to be similar, which demonstrates that the curvature-toggle-brace delivers the same damping as the curvature-brace, but with smaller damper size.

Damper force

The damper force is determined by equation (9), and the displacement of the damper with respect to the side-to-side mode, scaled according to a tower top displacement of 0.5 m. This is identical to the damper displacement shown in figure 7. Figure 10(a) shows the damper force as a function of θ_3 for a damper in a curvature-brace and figure 10(b) shows the damper force for a damper in a curvature-toggle-brace. The solid line in the figures corresponds to optimum viscous damping $\zeta = \zeta_{max}$, while the dashed line corresponds to a damping ratio half that of attainable damping $\zeta = \zeta_{max}/2$. As expected the damper force corresponding to optimum damping for a damper in a curvature-toggle-brace is significantly smaller than the damper force of a damper in curvature brace. Furthermore, due to the semicircular trajectory of the complex root in the complex plane, a damper system with a damping ratio half that of maximum attainable damping, only needs a damper force that is approximately one fourth of the damper force needed at optimum.

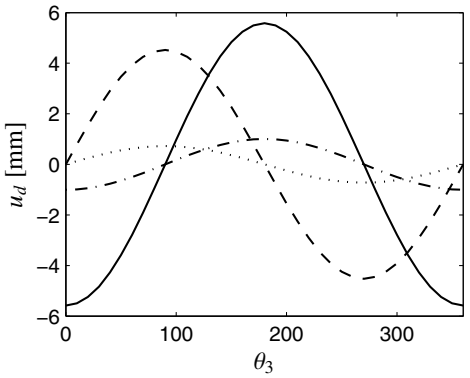

Fig. 7. u_d for the curvature brace with respect to the fore-aft mode (dotted) and the side-to-side mode (dash-dotted) and u_d for the curvature-toggle brace with respect to the fore-aft mode (dashed) and the side-to-side mode (solid)

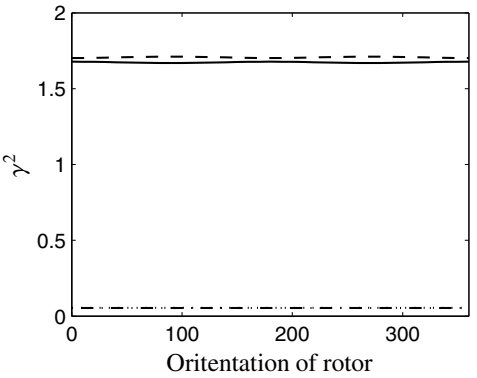

Fig. 8. γ^2 for six curvature-braces with respect to the fore-aft mode (dotted) and the side-to-side mode (dash-dotted) and u_d for six curvature-toggle braces with respect to the fore-aft mode (dashed) and the side-to-side mode (solid)

Time simulation in HAWC2

In order to further investigate the damping effect of installing passive dampers in curvature-toggle-braces in a wind turbine tower, a simple time simulation is carried out using the commercial code `HAWC2` [12]. `HAWC2` (Horizontal Axis Wind turbine simulation Code 2nd generation) is an aero-elastic code developed at DTU Wind Energy, which allows for dynamic simulations of wind turbines during operation. A model of the OC3 reference wind turbine is used for the time simulations. The model includes Rayleigh damping, equivalent to a damping ratio of $\zeta_u \simeq 0.0065$ for the first two tower modes. The brace members and the toggle mechanism are modeled directly in HAWC2, while the damper is modeled as an external system using a `dll` [13]. The curvature-toggle-brace system which is implemented in the HAWC2 model consist of six toggle-braces in a 60° configuration, equivalent to the system modeled with the simple beam model. The viscous damping parameter is tuned to optimum according to (21).

The wind turbine is again assumed at standstill. The structure is loaded by a single harmonic force acting at the waterline of the monopile, at an angle of 45° to the rotor direction, thus initiating both the fore-aft mode and the side-to-side mode. After some time the force is removed and the free decay is observed. Figure (11)(a) shows the tower

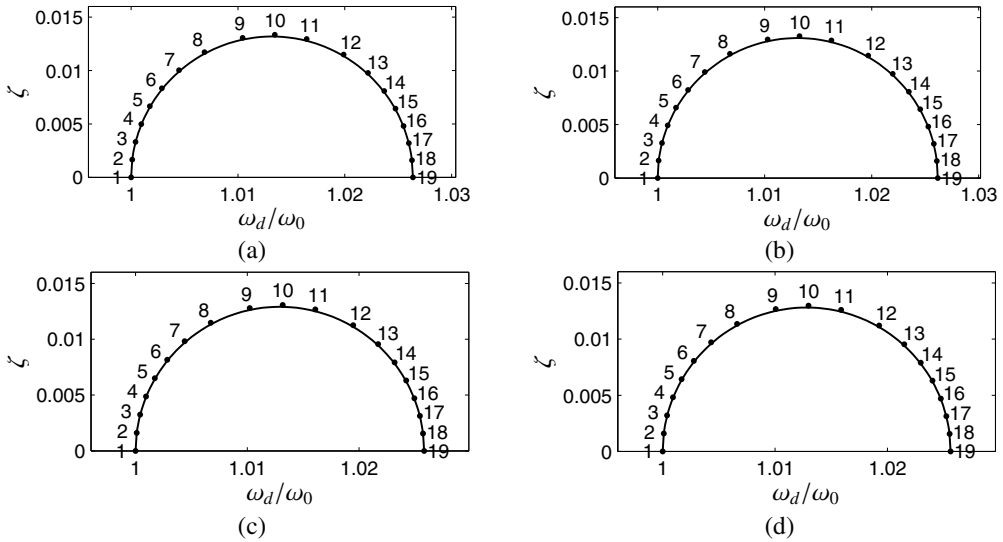

Fig. 9. Root locus associated with a curvature-brace system for (a) the fore-aft mode and (b) the side-to-side mode and root locus associated with a curvature-toggle-brace system for (c) the fore-aft mode and (d) the side-to-side mode

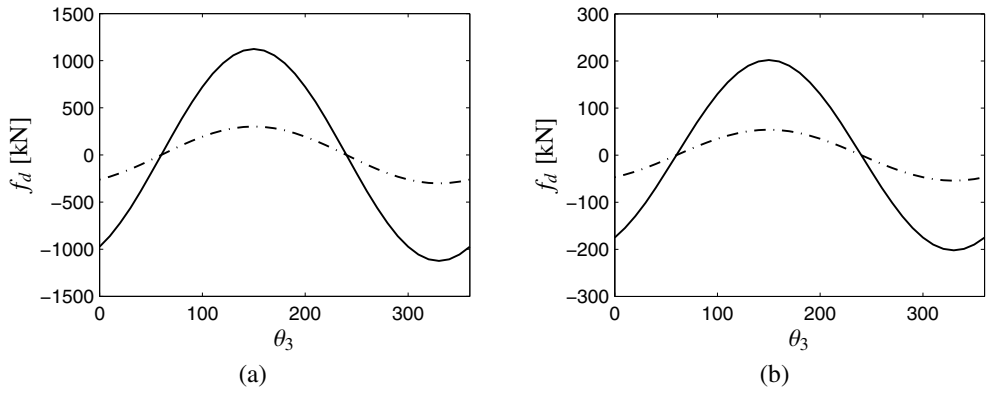

Fig. 10. Damper force as a function of θ_3 for the curvature-brace (a) and for the curvature-toggle-brace (b). The curves are for optimum damping $\zeta = \zeta_{max}$ (solid) and for a damping ratio half that of maximum attainable damping $\zeta = \zeta_{max}/2$ (dash-dotted)

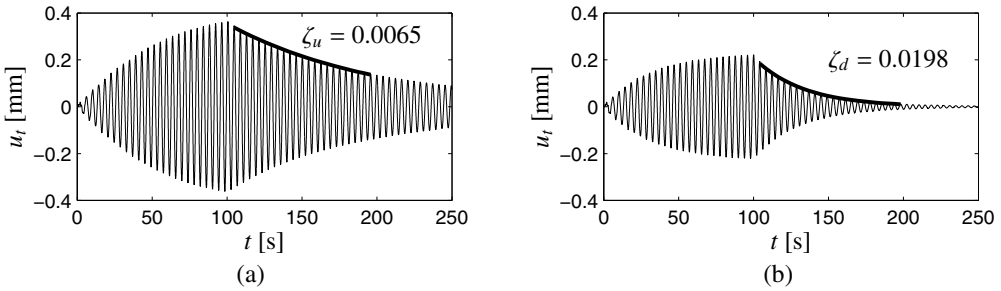

Fig. 11. Time simulation from HAWC2 without dampers (a) and with dampers (b)

top displacement for the wind turbine without external dampers, and figure (11)(b) shows the tower top displacement for the wind turbine with external dampers. The free decay is fitted with an exponential fit (solid line), from which an estimate of the damping ratio is computed. As expected the wind turbine with external dampers has the highest damping ratio. The difference in damping ratio between the two time simulations is $\Delta\zeta = \zeta_d - \zeta_u \simeq 0.013$, which corresponds well to the maximum attainable damping previously estimated by the simple beam model.

Conclusion

A new toggle-brace-damper concept for installing dampers at the bottom of fixed offshore wind turbines has been presented. Compared to a brace design where the damper is connected directly to the tower wall, the damper stroke is significantly increased, thereby increasing the feasibility of installing dampers inside the tower. In the numerical example presented a single circumferential row of toggle brace dampers is seen to increase the damping ratio of the two lowest tower modes by $\Delta\zeta = 0.013$. In a practical implementation 2-3 rows of dampers at different heights could be installed together in order to further increase attainable damping. As offshore wind turbines continue to increase in size and are moved to larger water depths, the toggle-brace-damper concept could become a feasible alternative to the tuned mass damper concept for damping of offshore wind turbine tower vibrations.

References

[1] Tarp-Johansen, N., Andersen, L., Christensen, E., Mørch, C., Frandsen, S., Kallesøe, B.. Comparing sources of damping of cross-wind motion. In: Proceedings of the European Wind Energy Conference & Exhibition. Stockholm, Sweden; 2009,.
[2] Colwell, S., Basu, B.. Tuned liquid column dampers in offshore wind turbines for structural control. Engineering Structures 2009;31(2):358–368.
[3] Lackner, M.A., Rotea, M.A.. Passive structural control of offshore wind turbines. Wind energy 2011;14(3):373–388.
[4] Fischer, T., Rainey, P., Bossanyi, E., Kühn, M.. Study on control concepts suitable for mitigation of loads from misaligned wind and waves on offshore wind turbines supported on monopiles. Wind Engineering 2011;35(5):561–574.
[5] Constantinou, M., Tsopelas, P., Hammel, W., Sigaher, A.. Toggle-brace-damper seismic energy dissipation systems. Journal of Structural Engineering 2001;127(2):105–112.
[6] Hwang, J.S., Huang, Y.N., Hung, Y.H.. Analytical and experimental study of the toggle-brace-damper systems. Journal of Structural Engineering 2005;131(7):1035–1043.
[7] Main, J., Krenk, S.. Efficiency and tuning of viscous dampers on discrete systems. Journal of Sound and Vibration 2005;286(1-2):97–122.
[8] Krenk, S.. A general format for curved and non-homogeneous beam elements. Computers & structures 1994;50(4):449–454.
[9] Svendsen, M., Krenk, S., Høgsberg, J.. Wind turbine rotors with active vibration control. Ph.D. thesis; DTU; 2011.
[10] Høgsberg, J.R., Krenk, S.. Linear control strategies for damping of flexible structures. Journal of Sound and Vibration 2006;293(1):59–77.
[11] Jonkman, J., Musial, W.. Offshore code comparison collaboration (OC3) for IEA task 23 offshore wind technology and deployment. Tech. Rep.; National Renewable Energy Laboratory; 2010. NREL/TP-500-48191.
[12] Larsen, T.J., Hansen, A.M.. How 2 HAWC2, the user's manual. Risø National Laboratory; 2007.
[13] Hansen, A.M., Larsen, T.J.. Gear dynamics. Tech. Rep.; Risoe National Lab.; 2009. Research in Aeroelasticity EFP-2007-II, Risoe-R-1698(EN):134-142.